Morphology-dependent singlet fission and photodegradation in functionalized tetracenes

Winston T. Goldthwaite[a], Evan Lambertson[a], Madalyn Gragg[a], Roshell Lamug[a], John Anthony[b], Oksana Ostroverkhova*[a]
[a]Dept.of Physics, Oregon State University, Corvallis, OR 97331
[b]Dept. of Chemistry, University of Kentucky, Lexington, KY 40506

ABSTRACT

Singlet fission (SF) is a charge carrier multiplication process that can occur in organic semiconductors and has potential to enhance (opto)electronic device performance. We examine how SF depends on molecular packing with functionalized tetracene (R-Tc) crystals which have the same monomer properties but different crystal packings with 'slip-stack' (R=TES) and 'gamma' (R=TBDMS) packing structures. Using temperature-dependent photoluminescence spectroscopy, we find that the triplet pair state (TT) in R-Tc systems under study is non-emissive, and the PL is dominated by that from low-energy emissive trap states in TES-Tc and from aggregate states in TBDMS-Tc, with the emissive channels competing with SF. We also study the effects of photodegradation from endoperoxide formation on R-Tc and the relationship between photodegradation and SF and find that the 'gamma'-packed TBDMS-Tc is more photostable than the 'slip-stacked' TES-Tc derivative. To analyze SF and competitive pathways, we constructed a 4-state kinetic model to reproduce the observed PL data, which predicts maximum SF free triplet yields of 190% for TES-Tc and 185% for TBDMS-Tc at room temperature.

Keywords: Organic semiconductors, singlet fission, optoelectronics, photodegradation

1. INTRODUCTION

Improving the performance of (opto)electronic devices such as photovoltaics is a major goal in semiconductor research. One promising way to enhance device performance is with singlet fission (SF), a charge-carrier multiplication process where one singlet exciton S1 is converted to two triplet excitons (T1) via a spin-entangled triplet pair state (TT) [1], $S1 \rightarrow TT \rightarrow 2T1$. This process occurs in organic semiconductors where double the T1 energy is approximately equal to the S1 state energy, $2E(T1) \approx E(S1)$. The dependence of intermolecular singlet fission on morphology is not well understood, and determining molecular packings conducive to SF is necessary to inform the design of SF materials and devices. Furthermore, singlet fission materials are susceptible to photodegradation reactions which decrease the performance. Understanding the relationship between photophysical and photochemical processes, and their dependence on morphology, is essential to realizing SF (opto)electronic devices. In this paper, we report on the morphology-dependent SF and photodegradation behavior of two functionalized tetracenes (R-Tc, R=TES, TBDMS), which are benchmark (opto)electronic and SF materials. Different side groups R alter the crystal packing structure of the material, without affecting monomer properties, allowing direct comparison of morphological effects between the 'slip-stack' packing of TES-Tc and 'gamma' packing of TBDMS-Tc. [2] Another R-Tc derivative, TIPS-Tc, has been extensively studied for its endothermic SF properties, but its crystal packing is not optimal for T1 generation. [3] We employed temperature-dependent photoluminescence (PL) spectroscopy (steady-state and time-resolved), kinetic modelling, and TD-DFT calculations to evaluate SF and competing processes in R-Tc crystals. [4] Here, we focus on the development of the kinetic model that adequately describes both steady-state and time-resolved PL data in the 1.6 K -300 K temperature range. We identify distinct emissive relaxation pathways competitive to SF, where 'slip-stack' TES-Tc has higher SF T1 yields, especially at temperatures below 150 K, from larger π- π overlaps and intermolecular coupling strengths compared to 'gamma' TBDMS-Tc. However, the 'gamma' TBDMS-Tc packing offers greater photostability, suggesting a trade-off between SF performance and photostability.

*oksana@science.oregonstate.edu, Telephone: 1 541 737 1679

Physical Chemistry of Semiconductor Materials and Interfaces XXIII, edited by Andrew J. Musser, Loreta A. Muscarella, Proc. of SPIE Vol. 13127, 131270B
 · 0277-786X · doi: 10.1117/12.3027820

2. MATERIALS AND METHODS

Crystals of R-Tc (side groups R=TES [(triethylsilyl)ethynyl] and R=TBDMS [(tert-butyldimethylsilyl)ethynyl]) were grown from dropcasting a 3-5 mM R-Tc in chlorobenzene solution onto a glass slide coated with a 50 nm Ag mirror in a 0 °C chiller. The slow evaporation of the solvent leaves behind a field of crystals, from which high-quality crystals were identified for measurements. X-ray diffraction (XRD) spectra were also taken, showing TES-Tc forms crystals in the (100) orientation, and TBDMS-Tc in (020) relative to the substrate, shown in Fig. 1. The TES-Tc single crystal has a triclinic structure with two molecules per unit cell (Z = 2) and unit cell parameters a = 11.83 Å, b = 12.38 Å, c = 13.2 Å, α = 64.02°, β = 72.39°, and γ = 63.99°. The TBDMS-Tc single crystal has a monoclinic structure with four molecules per unit cell (Z = 4) and unit cell parameters a = 6.90 Å, b = 32.67 Å, c = 13.32 Å, α = 90.0°, β = 98.22°, and γ = 90.0°.

Optical absorbance and photoluminescence (PL) spectroscopy were done on R-Tc crystals. For absorbance, the samples were illuminated by white light from tungsten lamp (Fiber-Lite DC-950), and spectra collected with a PI SpectraPro HRS 300 spectrograph. Steady-state PL measurements were taken with 532 nm cw excitation (Verdi-5, Coherent, Inc.), which was filtered by a 532 nm LP filter and spectra were collected the same as for absorbance. Photodegradation measurements were taken by continually illuminating the R-Tc crystal (with white light or 532 nm), and periodically measuring the spectra to track the evolution over time. Time-resolved PL lifetimes measurements (TCSPC) were taken using a 100 fs, 200 kHz 515 nm SHG from a 1030 nm fundamental (Pharos, Light Conversion), and the PL was collected and measured with an APD (MPD PDM) and TCSPC card (Picoquant TimeHarp 260) with an instrument response function (IRF) of 300 ps. Lifetimes of states τ were then found by fitting exponential decay functions to the measured PL decays. To study temperature-dependent PL behavior, R-Tc crystals were placed in a magneto-optic cryostat (Opticool, Quantum Design) which can probe from 1.6-300 K.

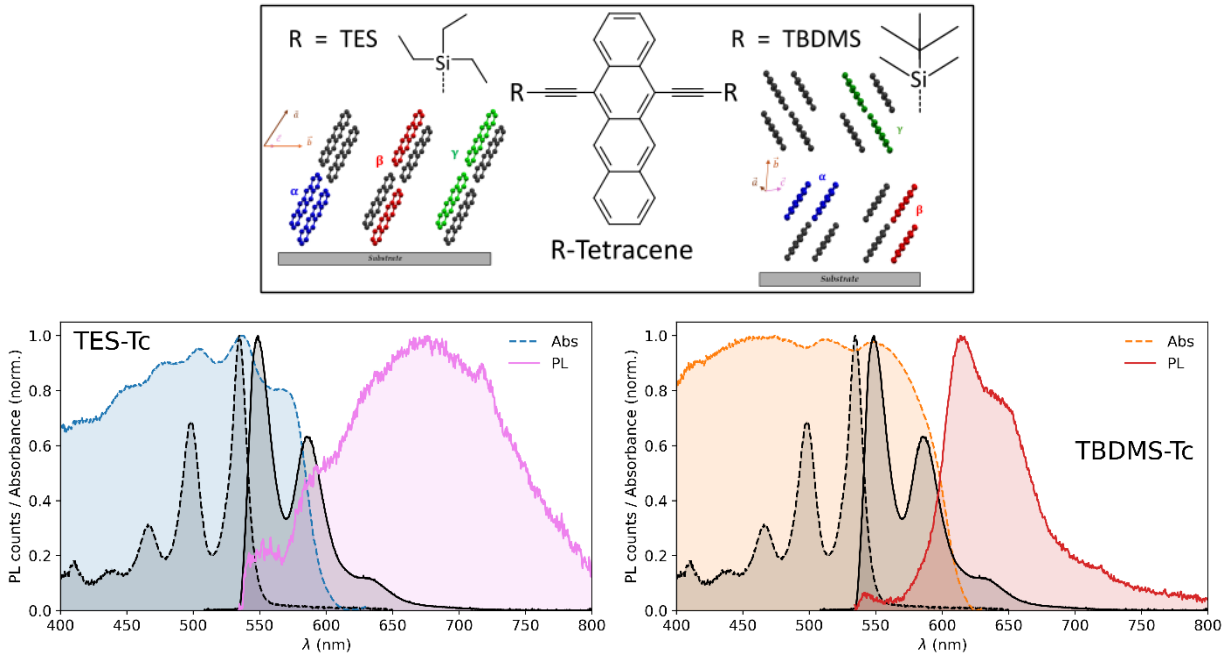

Figure 1. Top: Molecular structure of R-Tc and side groups R=TES/TBDMS with schematic of packing structure relative to substrate (colored molecules are nearest-neighbor dimer pairs). Bottom: Absorbance (dashed lines) and photoluminescence (PL) (solid lines) spectra of TES-Tc and TBDMS-Tc crystals, and dilute TES-Tc solution which shows monomer properties.

3. OPTICAL PROPERTIES

The steady-state absorbance and PL measurements on R-Tc solution and crystals are shown in Fig.1. Both absorption and PL spectra of R-Tc crystals show redshift from those of solution. The TBDMS-Tc crystals predominantly emit from an S1 aggregate ('S1agg') state at ~610 nm, and TES-Tc crystals from trap states ('Sx') at >650 nm. Similar emissive states have been observed in other functionalized acenes and SF materials, but there is not a consensus on the origin of these states, and whether this emission is due to TT states [3,5] or competitive to SF emissive states such as excimers [6,7]. At room temperature, both R-Tc crystals are relatively nonemissive, although TBDMS-Tc has higher PL yields than TES-Tc, suggesting that both crystals have highly efficient SF which reduces PL.

PL Temperature Dependence

To study the origin of these states and analyze SF in R-Tc, we measured temperature-dependent steady-state and time-resolved behavior of S1agg and Sx PL in R-Tc crystals from 1.6-300 K in Fig. 2. There is >100x increase in PL yield from both 'S1agg' and 'Sx' states from 300 K to 1.6 K, implying the presence of a thermally activated nonradiative process such as endothermic SF. This PL temperature dependence was analyzed as an Arrhenius process with rate constant $k = Ae^{-E_a/k_BT}$, where E_a is the activation energy and k_B is the Boltzmann constant. These fits revealed activation energies of 58 meV and 156 meV, for TBDMS-Tc and TES-Tc crystals, respectively. These values are consistent with activation energies for endothermic SF obtained from TIPS-Tc and bare Tc, which have been reported in the range of 50-200 meV [3]. Despite these differences between Sx and S1agg PL and in nature of these states, the overall temperature-dependent behavior is qualitatively similar. This suggests that there is another state or process mediating the observed behavior, such as TT states.

The time-dependent PL dynamics also show temperature dependence, but much weaker than the steady-state PL, with only an increase of ~10x between 300 K and 1.6 K for the Sx/S1agg states. Because both the temperature dependence for the PL yield and lifetimes are proportional to $(k_{rad} + k_{nonrad}(T))^{-1}$, where k_{rad} is the radiative decay rate and $k_{nonrad}(T)$ is the temperature dependent nonradiative decay rate, there must be an additional temperature-dependent process of formation of the emissive state so that PL ~ $\Phi_0(T)\, k_{rad}(k_{rad} + k_{nonrad}(T))^{-1}$ where $\Phi_0(T)$ is the probability of forming the emissive state. Φ_0 acquires temperature dependence from the temperature-dependent competing process of TT formation in SF. The TT formation occurs on picosecond time scales, which is too fast to observe in the PL dynamics limited by 300 ps IRF. To understand the excited-state dynamics in R-Tc and how it differs between these two derivatives, we built a kinetic model which recreates the observed PL data, discussed in Section 4.

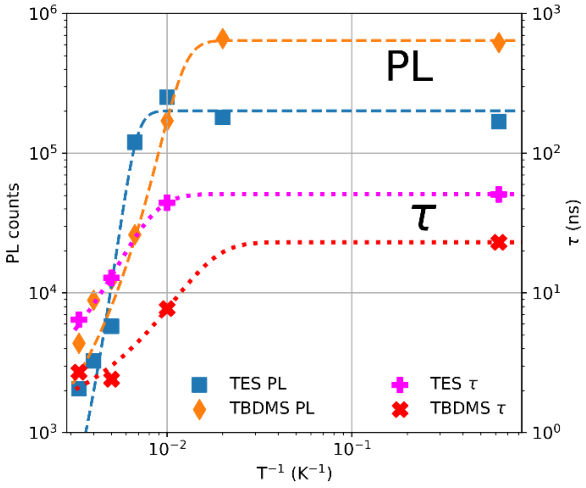

Figure 2. Temperature-dependent PL yields and lifetimes τ for Sx in TES-Tc crystals and S1agg in TBDMS-Tc crystals, from 1.6 K to 300 K. The PL yields increase by two orders of magnitude from 300 K to 1.6 K, whereas the lifetimes only have a one order of magnitude increase. Dashed lines are Arrhenius fits to the data, $PL, \tau \sim (k_0 + k_1 \exp(-E_a/k_BT))^{-1}$.

Photodegradation

One major drawback for (functionalized) acenes is their poor photostability, where tetracenes are particularly susceptible to endoperoxide (EPO) formation from reacting with singlet oxygen $^1O_2$. [8,9] Ground state oxygen is a triplet state ($^3O_2$), so T1 states generated via singlet fission can transfer energy to $^3O_2$ if E(T1)>0.98 eV, exciting it to form the highly reactive $^1O_2$. Because the T1 state in tetracenes is >1 eV [4,8], high SF yields can counterproductively increase EPO formation, causing faster degradation of the SF material. We investigated EPO formation in R-Tc crystals, with the integrated absorbance in the visible and PL evolving due to photodegradation in air shown in Fig. 3. The absorbance decays show that TBDMS-Tc crystals clearly have superior photostability, with a monoexponential decay time constant of 2500±100 s, compared to 400±20 s for TES-Tc under the same white-light illumination conditions. This could suggest that TES-Tc has higher SF yields to generate more T1, thus more $^1O_2$ and faster EPO formation.

In the PL evolution (inset of Fig. 3), the TBDMS-Tc crystal has a monotonic decrease in S1agg PL to about 60% of the initial yield. The remaining PL is from molecular populations not susceptible to EPO formation, either because the preceding degradation has destroyed SF pathways and T1 are no longer generated while other pathways of generating reactive oxygen species are considerably less efficient, or because these molecules are in locations in the crystal structure difficult for $^1O_2$ to reach. Interestingly, the TES-Tc crystal PL first increased by a factor of ~15, before decaying. This behavior was previously observed in other functionalized acenes as well, such as TIPS-Tc and TIPS-pentacene. [2,9] This PL increase is possible if the molecules which efficiently undergo SF are most susceptible to EPO formation, reducing SF yields, but increasing the yield of competitive pathways (e.g. Sx or S1 PL). The subsequent decay, however, indicates that there is a mechanism of generating reactive oxygen and forming EPOs from singlet states as well. [10] To help understand this behavior, we turn to a SF kinetic model which can predict T1 yields and analyze SF and competitive pathways.

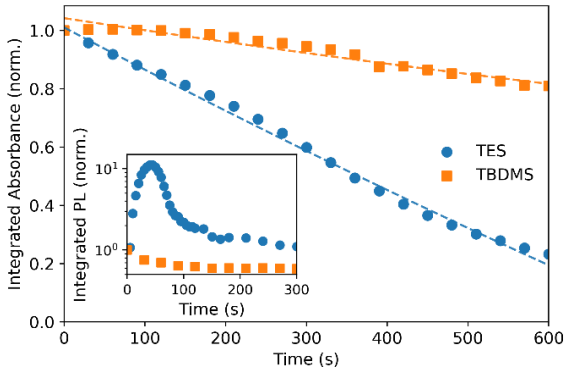

Figure 3. Photodegradation of absorbance and PL (inset) spectra of TES-Tc and TBDMS-Tc crystals undergoing EPO formation. Dashed lines are monoexponential decay fits with time constants of 400±20 s and 2500±100 s, respectively. The PL photodegradation behavior has opposite trends, where TES-Tc Sx PL increases by a factor of ~15 before decreasing, and TBDMS-Tc S1agg PL monotonically decreases to about 60% of the initial yield.

4. KINETIC MODEL

To evaluate the SF process in R-Tc crystals, we constructed a kinetic model to analyze the PL steady-state and time-resolved spectroscopy data. [11] We began by using the simplest possible model to describe the data, and added complexity as needed to improve accuracy. The time-dependent model solution was found by giving an initial condition of S1 population of 1 and all other states 0 (i.e. direct S1 excitation) and using Mathematica NDSolve to evaluate the set of coupled differential equations. The steady state solution was found by directly solving the coupled equations with the derivatives set to 0 if possible, and otherwise found by including an S1 generation term $G = 1$ ns^{-1} to $dN1/dt$ in the model, and using Mathematica Minimize to find populations which minimize the derivatives of each (directly setting the differential equations to 0 can give trivial solutions). Rates were first chosen by taking values from comparable systems in the literature or from fits to the PL lifetime decays, then adjusted within physically reasonable limits to improve agreement of the model solution with the data.

3-State Model

Initially, we attempted to fit the data with a 3-state model consisting of S1, TT, and T1 (Eqs. 1), where the observed PL would be direct emission from TT, and TT → 2T1 dissociation is a thermally activated process with rate $k_2(T) = k_2^a + k_2^b e^{-E_2/k_BT}$, where E_2 is the activation energy. This model fails to reproduce the observed dynamics, particularly the bi/triexponential behavior of the PL decays at high temperatures, as shown in Fig. 4 with parameters in Table 1. This model also results in an enhancement in steady-state PL yield at 1.6 K by less than an order of magnitude compared to 300 K PL yield (inset of Fig. 4), rather than over 2 orders of magnitude as observed in the PL data (Fig. 2). However, one key observation from this iteration of the model was the importance of including triplet fusion (TT → S1). This reverse SF process is essential in the next iterations of the model as it kinetically links TT behavior to Sx/S1agg PL behavior and explains the similar properties of both states despite different origins.

$$\text{S1: } \frac{dN1}{dt} = -(k_{12} + k_1)N1 + k_{21}N2 \tag{1}$$

$$\text{TT: } \frac{dN2}{dt} = k_{12}N1 - (k_{21} + k_2(T))N2$$

$$\text{T1: } \frac{dN3}{dt} = 2k_2(T)N2$$

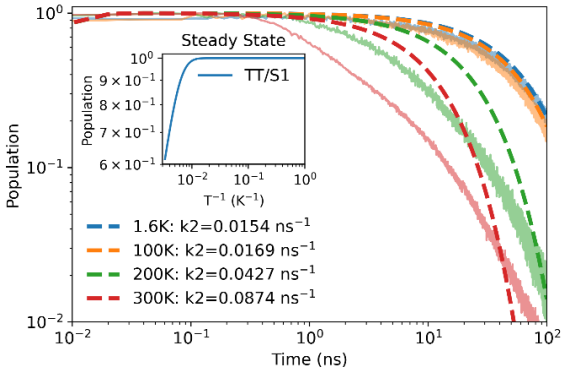

Figure 4. Time-dependent solution to 3-state kinetic model (S1/TT/T1) to TES-Tc with temperature-dependent TT → 2T1 rate (k_2) for parameters in Table 1. Solid lines are measured PL lifetimes decays for the Sx state, overlaid with dashed lines showing the Sx population calculated from the model. Inset shows the steady-state TT/S1 population ratio. The model agrees well with the low-temperature monoexponential decays but fails to recreate high-temperature dynamics and steady state results.

Table 1. Parameters used in the 3-state kinetic model solution shown in Fig. 4.

TES-Tc 3 State Kinetic Model Parameters					
k_{12} (ns^{-1})	k_1 (ns^{-1})	k_{21} (ns^{-1})	k_2^a (ns^{-1})	k_2^b (ns^{-1})	E_2 (meV)
200	1/20	1/10	1/65	1/2	50

4-State Model

To account for these discrepancies, the next iteration of the model included a 4th state, representing Sx/S1agg (Eqs. 2), which has a thermally activated PL emission rate $k_3(T)$, in addition to $k_2(T)$ for TT → 2T1, motivated by the temperature-dependence of Sx PL upon direct 633 nm cw excitation [4]. This also means that if the TT state itself is nonemissive, the dark TT dynamics can still be reflected in the Sx/S1agg PL because these states are kinetically linked. We investigated Sx/S1agg behavior when populated from S1, TT, or both, and found that including only S1 → Sx/S1agg is necessary. Having a TT ⇋ Sx/S1agg pathway reduces model accuracy and was omitted. The PL decays could be accurately recreated with this model for both TBDMS-Tc and TES-Tc as shown in Fig. 5 with parameters in Table 2. However, like in the previous iteration, the steady state PL temperature dependence is much weaker (insets of Fig. 5) than what was measured (Fig. 2). Attempting to use parameters to match the steady-state data instead of the dynamics has the same effect, where

the steady-state behavior can be recreated, but then the dynamics are not accurate across the whole temperature range used in our experiments. For both the steady-state and dynamics to match the model, a 3rd temperature dependence is included on S1 → TT ($k_{12}(T)$), which introduces the temperature dependent probability of formation of the emissive state (Φ_0) discussed above. This is expected to occur on faster timescales than our IRF time resolution, thus this is the possible picosecond time-scale temperature dependent process described in the previous section which could quantitatively describe both the steady-state and the dynamics.

$$\text{S1: } \frac{dN1}{dt} = -(k_{12} + k_{13} + k_1)N1 + k_{21}N2 \tag{2}$$

$$\text{TT: } \frac{dN2}{dt} = k_{12}N1 - (k_{21} + k_2(T))N2$$

$$\text{Sx/S1agg: } \frac{dN3}{dt} = k_{13}N1 - k_3(T)N3$$

$$\text{T1: } \frac{dN4}{dt} = 2k_2(T)N2$$

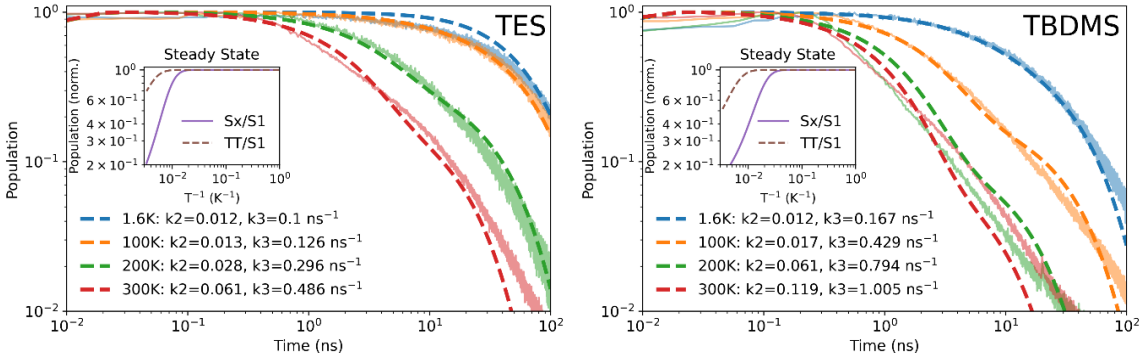

Figure 5. Time-dependent solution to 4-state (S1/TT/Sx(S1agg)/T1) kinetic model to TES-Tc and TBDMS-Tc with temperature-dependent TT → 2T1 (k_2) and Sx/S1agg PL (k_3) for parameters in Table 2. Solid lines are measured PL lifetimes decays for the Sx/S1agg state, overlayed with dashed lines showing the Sx/S1agg population calculated from the model. Insets show the steady-state TT/S1 and Sx/S1 population ratios.

Table 2. Parameters used in the 4-state kinetic model solution shown in Fig. 5. Activation energies are E_2 = 60 meV/40 meV, E_3 = 35 meV/15 meV, for TES-Tc/TBDMS-Tc.

4-State Kinetic Model Rates 1								
ns^{-1}	k_1	k_{12}	k_{21}	k_{13}	k_2^a	k_2^b	k_3^a	k_3^b
TES	1/20	200	1/10	10	1/80	1/2	1/10	3/2
TBDMS	1/20	200	1/10	45	1/80	1/2	1/6	3/2

The final 4-state kinetic model solution is shown in Fig. 6 with parameters in Table 3. The temperature dependence on S1 → TT (k_{12}) primarily affects the steady-state population, where higher k_{12} depopulates S1 faster and generates more TT states. This results in an increased SF yield, but a decrease in the steady-state PL. Because the S1 → TT rate is faster than all other processes considered in the model, and so much faster than the observed PL dynamics, k_{12} has a negligible effect on the time-dependent model solution. Tuning these three temperature dependent rates (k_{12}, k_2, k_3) gives qualitatively correct results for steady state and time-dependent Sx/S1agg PL, except for the long decay component at high temperatures. At 300 K, both the Sx and S1agg decays from the model are much shorter than what was measured. This could be explained by triplet-triplet annihilation (TTA) from T1+T1 recombination, which can account for delayed PL because it repopulates emissive states (directly or indirectly) at longer timescales. It could also be expected to be temperature dependent due to thermally activated exciton diffusion and contribute appreciably only at high temperatures (>200 K). TTA was neglected from the model because including transitions from the T1 population (which is treated as a reservoir in the model) adds significant complexity and may require a different initial approach to appropriately include. As such, we report the most

accurate results using the simplest model. This model predicts an upper limit on SF quantum yield (T1 generated per S1) of 190% for TES-Tc, and 185% for TBDMS-Tc at 300 K, with significant differences in T1 generation between TES-Tc and TBDMS-Tc occurring only below 150 K where the 'slip-stack' packing of TES-Tc is advantageous for TT formation and dissociation. [4] Given that the maximal T1 yields at 300 K are similar in TES-Tc and TBDMS-Tc, it is interesting that the TBDMS-Tc is about a factor of 6 times more stable than TES-Tc in air (Fig. 3), and it indicates that it is possible to design a highly efficient SF system, at least within a temperature range practical for optoelectronic devices, without sacrificing photostability.

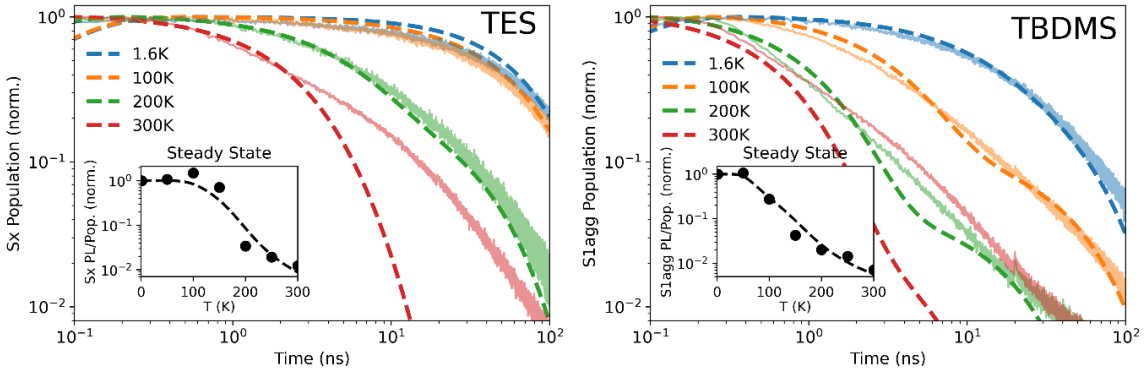

Figure 6. Time-dependent solution to 4 state (S1/TT/Sx(S1agg)/T1) kinetic model to TES-Tc and TBDMS-Tc with temperature-dependent S1 → TT (k_{12}), TT → 2T1 (k_2), and Sx/S1ag PL (k_3) with parameters in Table 3. Lines are measured PL lifetimes decays for the Sx/S1agg state, overlayed with dashed lines showing the Sx/S1agg population calculated from the model. Inset shows the steady-state Sx/S1agg population from model (dashed lines) against the total PL yield data as a function of temperature, normalized to 1.6 K values.

Table 3. Parameters used in the final 4-state kinetic model solution shown in Fig. 6. Activation energies are E_{12} = 65 meV/50 meV, E_2 = 130 meV/80 meV, E_3 = 50 meV/25 meV, for TES-Tc/TBDMS-Tc.

4-State Kinetic Model Rates 2									
ns^{-1}	k_1	k_{21}	k_{13}	k_{12}^a	k_{12}^b	k_2^a	k_2^b	k_3^a	k_3^b
TES	1/10	1/20	5	10	500	1/100	5	1/10	4
TBDMS	1/10	1/20	3	10	500	1/100	40	1/20	3

5. CONCLUSIONS

We analyzed excited-state dynamics in 'gamma' packed TBDMS-Tc and 'slip-stack' packed TES-Tc using temperature-dependent PL spectroscopy and kinetic modelling. Our findings highlight key differences in the photophysics and photochemistry of these materials resulting from their morphological differences. The 4-state kinetic model shows that the emissive states are a competitive relaxation process to SF, and the TT states in these R-Tc are nonemissive. The model shows that Sx/S1agg and TT states do not need to have a direct transition, and TT/SF properties are imparted on the emissive states via triplet fusion TT → S1→ Sx/S1agg. Although TES-Tc and TBDMS-Tc have comparable SF yields at room temperature, at 190% and 185%, respectively, TES-Tc has superior SF T1 yields at low temperatures (<150 K) due to higher π-π interactions between molecules. However, the superior SF performance of 'slip-stack' packing is detracted by its poor photostability, with 6x faster photodegradation from EPO formation than in TBDMS-Tc 'gamma' packing at room temperature. Nevertheless, our findings show that it is possible to achieve high SF yields, at least in a limited temperature range, without sacrificing photostability with an appropriate packing morphology.

ACKNOWLEDGEMENTS

This work was supported by the National Science Foundation (CHE-1956431). Sample fabrication and characterization was partially performed in NSF-funded user facilities via NNCI:NNI EECS-2025489 and MRI DMR-1920368 grants.

REFERENCES

[1] Musser, A. J. and Clark, J., "Triplet-Pair States in Organic Semiconductors," Annu. Rev. Phys. Chem. 70(1), 323-351 (2019). https://doi.org/10.1146/annurev-physchem-042018-052435

[2] Goldthwaite, W., Chase, M., Gragg, M., Lamug, R., Windemuller, D., Parkin, S., Anthony, J. E., and Ostroverkhova, O., "Elucidating photophysics-photochemistry relationship in singlet fission materials," MRS Adv. 9, 707–714 (2024). https://doi.org/10.1557/s43580-024-00797-1

[3] Stern, H. L., et al., "Vibronically coherent ultrafast triplet-pair formation and subsequent thermally activated dissociation control efficient endothermic singlet fission," Nature Chem. 9, 1205-1212 (2017). https://doi.org/10.1038/nchem.2856

[4] Goldthwaite, W. T., Lambertson, E., Gragg, M., Anthony, J. E., Zuehlsdorff, T. and Ostroverkhova, O., "Morphology-Dependent Singlet Fission and Photodegradation in Functionalized Tetracene Crystals and Films," *Submitted*, (2024).

[5] Bayliss, S. L., et al., "Site-selective measurement of coupled spin pairs in an organic semiconductor," PNAS 115(20), 5077-5082 (2018). https://doi.org/10.1073/pnas.1718868115

[6] Dover, C., et al., "Endothermic singlet fission is hindered by excimer formation," Nature Chem. 10, 305-310 (2018). https://doi.org/10.1038/nchem.2926

[7] Huang, Y., et al., "Competition between triplet pair formation and excimer-like recombination controls singlet fission yield," Cell Rep. Phys. 2(2), (2021). https://doi.org/10.1016/j.xcrp.2021.100339

[8] Fudickar, W. and Torsten, L., "Why Triple Bonds Protect Acenes from Oxidation and Decomposition," J. Am. Chem. Soc. 134(36), 15071-15082 (2012). https://doi.org/10.1021/ja306056x

[9] Puro, R., van Schenck, J. D. B., Center, R., Holland, E. K., Anthony, J. E. and Ostroverkhova, O., "Exciton Polariton-Enhanced Photodimerization of Functionalized Tetracene," J. Phys. Chem. C 125(49), 27072-27083 (2021). https://doi.org/10.1021/acs.jpcc.1c06881

[10] Stuart, A. N., Wee, T. K. and Huang, D. M., "Role of Singlet and Triplet Excited States in the Oxygen-Mediated Photophysics and Photodegradation of Polyacenes," J. Am. Chem. Soc. 146(3), 2174-2186 (2024). https://doi.org/10.1021/jacs.3c12245

[11] Cruz, C.D., Chronister, E. L. and Bardeen, C. J., "Using temperature dependent fluorescence to evaluate singlet fission pathways in tetracene single crystals," J. Chem. Phys. 153(23), 234504 (2020). https://doi.org/10.1063/5.0031458